Locating Phospholamban in Co-Crystals with Ca^{2+}-ATPase by Cryoelectron Microscopy

Howard S. Young,* Larry R. Jones,† and David L. Stokes*
*Skirball Institute of Biomolecular Medicine, Department of Cell Biology, New York University School of Medicine, New York, New York; and †Krannert Institute of Cardiology, Indiana University Medical School, Indianapolis, Indiana USA

ABSTRACT Phospholamban (PLB) is responsible for regulating Ca^{2+} transport by Ca^{2+}-ATPase across the sarcoplasmic reticulum of cardiac and smooth muscle. This regulation is coupled to β-adrenergic stimulation, and dysfunction has been associated with end-stage heart failure. PLB appears to directly bind to Ca^{2+}-ATPase, thus slowing certain steps in the Ca^{2+} transport cycle. We have determined 3D structures from co-crystals of PLB with Ca^{2+}-ATPase by cryoelectron microscopy of tubular co-crystals at 8–10 Å resolution. Specifically, we have used wild-type PLB, a monomeric PLB mutant (L37A), and a pentameric PLB mutant (N27A) for co-reconstitution and have compared resulting structures with three control structures of Ca^{2+}-ATPase alone. The overall molecular shape of Ca^{2+}-ATPase was indistinguishable in the various reconstructions, indicating that PLB did not have any global effects on Ca^{2+}-ATPase conformation. Difference maps reveal densities which we attributed to the cytoplasmic domain of PLB, though no difference densities were seen for PLB's transmembrane helix. Based on these difference maps, we propose that a single PLB molecule interacts with two Ca^{2+}-ATPase molecules. Our model suggests that PLB may resist the large domain movements associated with the catalytic cycle, thus inhibiting turnover.

INTRODUCTION

The cycle of muscle contraction/relaxation is controlled by the release and reuptake of Ca^{2+} from the sarcoplasmic reticulum (SR). Ca^{2+} reuptake is accomplished by the ATP-dependent pump, Ca^{2+}-ATPase, which in cardiac and smooth muscle is regulated by phospholamban (PLB; Kirchberger et al., 1974; Tada et al., 1974). PLB interacts with the pump and lowers its apparent affinity for Ca^{2+} (Simmerman and Jones, 1998); this inhibition is relieved by β-adrenergic stimulation in a mechanism involving phosphorylation of PLB at Ser^{16} by protein kinase A. Under physiological conditions (e.g., exercise), this phosphorylation is the predominant mechanism underlying increases in the rate of cardiac relaxation and in SR Ca^{2+} loading (Luo et al., 1994). However, chronic Ca^{2+}-ATPase inhibition by PLB has been linked to SR dysfunction in human and animal heart failure (Sordahl et al., 1973; Meyer et al., 1995; Hasenfuss, 1998; Whitmer et al., 1988; Minmamisawa et al., 2000).

The SR Ca^{2+}-ATPase is a member of the family of P-type cation pumps, all of which form a phosphorylated intermediate during the catalytic cycle. Experimental evidence has long suggested that large conformational changes couple the formation of this phosphoenzyme to translocation of ions across the membrane. Such evidence includes changes in proteolytic cleavage, spectroscopic signals, chemical reactivity, and cross-linking (Jorgensen and Andersen, 1988). The structures of Ca^{2+}-ATPase from rabbit skeletal muscle (Zhang et al., 1998) and H^+-ATPase from *Neurospora* (Auer et al., 1998) revealed the conformational change induced by ion binding (Stokes et al., 1999) and the disposition of the 10 transmembrane helices. More recently, the atomic structure of the Ca^{2+}-bound (E_1) conformation of Ca^{2+}-ATPase (Toyoshima et al., 2000) revealed the domain architecture and overall fold. The three cytoplasmic domains are connected by flexible links and appear to be capable of independent motion during conformational changes. Comparison with the Ca^{2+}-free (E_2) conformation from cryoelectron microscopy (Zhang et al., 1998) indicates that these three cytoplasmic domains do in fact undergo large-scale, coordinated movements, which are somehow linked to the transmembrane helices involved in transporting the two Ca^{2+} ions.

Enzyme kinetic studies have demonstrated that PLB slows one or more steps in the Ca^{2+}-ATPase reaction cycle. In particular, different studies have implicated the conformational change following binding of the first Ca^{2+} ion ($E_1Ca \rightarrow E_1'Ca$; (Cantilina et al., 1993) and phosphoenzyme decomposition (E_2-P $\rightarrow E_2$; (Sasaki et al., 1992; Antipenko et al., 1997). Presumably, these inhibitory effects are mediated by direct physical interactions between Ca^{2+}-ATPase and PLB. In fact, specific interaction sites have been identified in the cytoplasmic domains (James et al., 1989; Toyofuku et al., 1993, 1994) and transmembrane domains (Kimura et al., 1996, 1997; Asahi et al., 1999; Cornea et al., 2000; Autry and Jones, 1997) of each protein.

Although the structure and stoichiometry of the PLB/Ca^{2+}-ATPase inhibitory complex are uncertain, a wide variety of studies suggest that there is a dynamic exchange between PLB monomers and pentamers. Mutagenesis of the PLB transmembrane domain indicates that monomeric PLB is a more effective inhibitor of Ca^{2+}-ATPase than pentameric PLB (Kimura et al., 1996, 1997; Asahi et al., 1999; Cornea et al., 2000; Autry and Jones, 1997). Furthermore,

Received for publication 20 December 2000 and in final form 6 May 2001.
Address reprint requests to Dr. David L. Stokes, Skirball Institute 3-13, NYU Medical Center, 540 First Ave., New York, NY 10016. Tel.: 212-263-1580; Fax: 212-263-1580; E-mail: stokes@saturn.med.nyu.edu.

0006-3495/01/08/884/11 $2.00

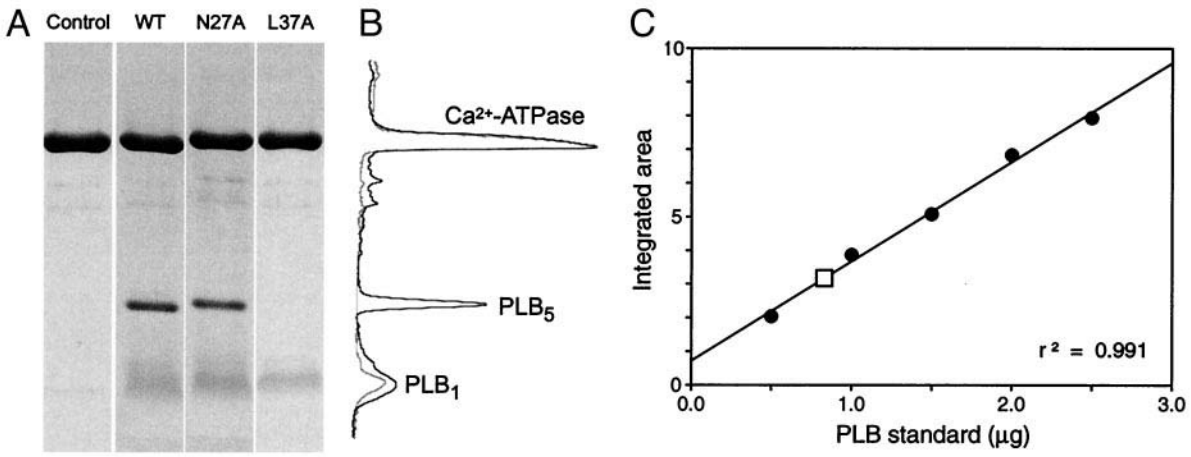

FIGURE 1 (*A*) Quantitation of Ca^{2+}-ATPase and PLB stoichiometry in reconstituted proteoliposomes used for crystallization. Co-reconstituted samples were run on a 6–20% gradient gel; *control* corresponds to reconstituted, purified Ca^{2+}-ATPase; WT, N27A, and L37A correspond to samples characterized in Tables 1 and 2. (*B*) Densitometer traces of the N27A (*black line*) and L37A (*gray line*) gel lanes shown in (*a*). (*C*) Standard curve generated from purified PLB_{L37A} run in adjacent lanes (*filled circles*) used for quantitation of the L37A gel lane (*open square*) shown in (*a*); the solid line represents a linear regression to the standard data.

phosphorylation of PLB, which reverses this inhibition, produces a larger proportion of PLB pentamers (Cornea et al., 1997). These results are consistent with a mechanism in which monomeric PLB interacts with and inhibits Ca^{2+}-ATPase; pentameric PLB is postulated to be inactive and phosphorylation to influence the distribution between these inhibitory and inactive states (Kimura et al., 1997; Stokes, 1997). However, this mechanism may be an oversimplification, given that a heterogeneous population of oligomers is almost always observed, and that residues interacting with Ca^{2+}-ATPase appear to be accessible even in the pentamer.

In this report, recombinant PLB representing different oligomeric species has been co-reconstituted with Ca^{2+}-ATPase under conditions suitable for tubular crystallization (Young et al., 1997, 1998). In particular, the Asn^{27} to Ala (N27A) and Leu^{37} to Ala (L37A) mutants were chosen based on their differing oligomeric properties. Both inhibit Ca^{2+}-ATPase to a greater extent than wild-type (WT), but L37A runs exclusively as a monomer and N27A runs predominantly as a pentamer in SDS gels. After co-reconstitution, we have used frozen-hydrated electron microscopy and helical image reconstruction to solve the structures of Ca^{2+}-ATPase reconstituted with WT PLB, L37A, or N27A. Comparison with previous structures of Ca^{2+}-ATPase alone revealed extra density, which we have assigned to the cytoplasmic domain of PLB and used to build a tentative structural model for the inhibitory complex.

MATERIALS AND METHODS

Reconstitution of PLB and Ca^{2+}-ATPase

Skeletal muscle SR vesicles were prepared from rabbit hind leg (Eletr and Inesi, 1972). Ca^{2+}-ATPase was purified from these SR vesicles by Reactive Red 120 affinity chromatography (Stokes and Green, 1990). Recombinant PLB mutants were expressed in Sf21 insect cells using the baculovirus system, and purified by monoclonal antibody affinity chromatography (Reddy et al., 1995).

Reconstitution was achieved following method II of Reddy et al. (1995), modified for the low lipid-to-protein ratios required for crystallization (Young et al., 1997). Purified, recombinant PLB was treated with Biobeads SM2 (Bio-Rad Laboratories, Hercules, CA) to remove the octylglucoside, and was lyophilized. Trifluoroethanol and chloroform were added to the lyophilized PLB, followed by the addition of an optimal mixture of egg yolk phosphatidylcholine, phosphatidyl ethanolamine, and phosphatidic acid (8:1:1 weight ratio) also in chloroform. The solvents were evaporated under dry nitrogen to yield a thin film of lipid and PLB on the wall of the tube. This thin film was lyophilized to completely remove residual solvent. Buffer (20 mM imidazole, pH 7.0; 100 mM KCl; 3 mM NaN_3) and detergent ($C_{12}E_8$) were added to resuspend the lipid/PLB film, followed by the addition of purified Ca^{2+}-ATPase yielding a weight ratio of 1 Ca^{2+}-ATPase/1 lipid/2 detergent. The detergent was removed by the addition of SM2 Biobeads with stirring at room temperature for 4 h (Levy et al., 1990a, b), with the rate of detergent removal controlled by the regimen of Biobead addition (Young et al., 1997). Finally, sucrose density gradient centrifugation was used to purify the reconstituted proteoliposomes that were subsequently used for crystallization. Ratios of Ca^{2+}-ATPase to PLB within these proteoliposomes were determined by SDS-PAGE (Fig. 1, Table 1). In particular, incremental amounts of purified PLB and Ca^{2+}-ATPase were run next to the proteoliposomes on a given gel. After Coomassie staining, gels were digitized with a Molecular Dynamics personal densitometer SI (Sunnyvale, CA) and bands were quantitated, after background subtraction, with the associated ImageQuant analysis software. Lanes with purified protein were used to create separate standard curves for Ca^{2+}-ATPase and PLB, from which the amount of each protein in proteoliposomes was estimated. The monomeric PLB species (L37A) was reconstituted to yield a final molar ratio of 1 PLB/1 Ca^{2+}-ATPase, and the pentameric PLB species (WT and N27A) were co-reconstituted to yield a final molar ratio of 3.5–5 PLB/1 Ca^{2+}-ATPase. ATPase activity was measured at 25°C or 37°C by a coupled enzyme assay (Warren et al., 1974), with EGTA-buffered Ca^{2+} concentrations of 0.15 μM and 4.0 μM (Fabiato and Fabiato, 1979). Concentrations of purified Ca^{2+}-ATPase were determined by the modified Lowry method (Lowry et al., 1951; Markwell

TABLE 1 Co-reconstitution of Ca^{2+}-ATPase and PLB

	Molar Stoichiometries		Normalized ATPase Activity			
			4.0 μM Ca^{2+}		0.15 μM Ca^{2+}	
	Lipid*	PLB†	−Ab‡	+Ab	−Ab	+Ab
Control	90	0	1.0§	0.93 ± 0.04 (n = 2)	0.34 ± 0.03 (n = 17)	0.34 ± 0.03 (n = 2)
PLB_{WT}	130	5 (8)	0.95 ± 0.16 (n = 12)		0.12 ± 0.03 (n = 12)¶	
PLB_{N27A}	130	3.5 (5)	1.04 ± 0.36 (n = 3)		0.08 ± 0.04 (n = 3)¶	
PLB_{L37A}	100	1 (2)	0.81 ± 0.11 (n = 7)	0.89 ± 0.04 (n = 2)	0.05 ± 0.02 (n = 7)¶	0.46 ± 0.13 (n = 2)

*Lipid/protein molar ratio after purification of proteoliposomes. In all cases the initial molar ratio was 150.
†PLB/Ca^{2+}-ATPase molar ratio after purification of proteoliposomes; initial ratios are shown in parentheses.
‡Anti-PLB monoclonal antibody 2D12, which mimics the effect of PLB phosphorylation (Briggs et al., 1992; Cantilina et al., 1993; Morris et al., 1991; Sham et al., 1991; Reddy et al., 1996).
§ATPase activities have been normalized relative to control reconstitutions performed simultaneously and assayed at 4.0 μM calcium. Average control activity at 4.0 μM calcium and 25°C was 4.22 ± 0.19 μmol/min/mg (n = 17). Errors correspond to SEM.
¶Statistically significant differences relative to the control with $p < 0.001$.

et al., 1978) and the micro BCA method (Pierce, Rockford, IL). Purified PLB concentrations were determined by the Amido black assay (Reddy et al., 1999). Lipid was estimated by a colorimetric determination of phosphorous, which is based on forming a phosphomolybdate complex (Chen et al., 1956; Chester et al., 1987).

Tubular crystallization

The proteoliposomes were collected by centrifugation, resuspended in buffer, and centrifuged again to wash away sucrose. To this pellet was added crystallization buffer containing 20 mM imidazole, pH 7.4; 100 mM KCl; 5 mM $MgCl_2$; 0.5 mM EGTA; and 0.5 mM Na_3VO_4 (Dux and Martonosi, 1983). In the cases of PLB_{WT}, PLB_{L37A}, and $Control_{TG}$, stoichiometric levels of thapsigargin (TG) were added to this solution to promote formation of tubular crystals (Sagara et al., 1992; Young et al., 2001). Dansylated thapsigargin (DTG) 30 μM was added for $Control_{DTG}$ as previously described (Zhang et al., 1998; Young et al., 2001). The pellet was subjected to two freeze-thaw cycles (freezing in liquid N_2, thawing in hand), was gently resuspended at 1–2 mg/ml with a micropipette, followed by two additional freeze-thaw cycles. Reconstituted samples were incubated at 15°C for 12 h, then shifted to 0°C for several days to two weeks, whereas Control samples were kept at 0°C for the entire time. Although crystallization occurred quickly, four to seven days were required for the highest frequency of tubular crystals.

Electron microscopy

Frozen-hydrated specimens were prepared by diluting crystals 20-fold with excess crystallization buffer, and then by applying 5 μl to 300-mesh copper grids that had been coated with perforated carbon films and glow-discharged in air. After blotting excess solution from the carbon side of the grids, they were immediately vitrified in an ethane slush and were stored in liquid N_2. Images of frozen-hydrated samples were obtained with a Philips (Eindhoven, Holland) CM200 FEG electron microscope equipped with an Oxford (Oxford, UK) CT-3500 specimen holder, which maintained the specimen temperature at −185°C. Images were recorded on Kodak SO163 film at 0.6–2.0 μm underfocus and at 50,000× magnification, with doses of 10–16 electrons/Å^2.

Image processing

Images of straight tubes suspended over holes in the carbon film were selected by optical diffraction and were digitized either with a PDS 1010 GM microdensitometer (Orbital Sciences Corp., Pomona, CA) at 13 μm intervals (2.534 Å pixel size) or with a Zeiss Scai (Carl Zeiss GMBH, Oberkochen, Germany) at 14 μm intervals (2.729 Å pixel size). Like other membranous tubes, co-crystals of PLB and Ca^{2+}-ATPase have a variable helical symmetry characterized by Bessel orders (n) of the principal (1, 0) and (0, 1) layer lines (Fig. 2, Toyoshima and Unwin, 1990). After determining these parameters, established procedures (DeRosier and Moore, 1970; Toyoshima and Unwin, 1990) were used for determining repeat distances, orientational parameters, twofold phase origins, and for extracting and averaging layer line data. The averaged data served as references for correcting crystal distortions (Beroukhim and Unwin, 1997). Briefly, individual repeat lengths of a tubular crystal were divided into short segments (~1000 Å) and independent orientational parameters were determined for each section. The contrast transfer function (CTF) of individual tubes was estimated using the programs of Tani et al. (1997) assuming 4.6% amplitude contrast (Toyoshima et al., 1993). The phases were corrected for the CTF before averaging layer line data, and the CTF amplitudes were used as weights during final data averaging and before Fourier-Bessel transformation (Unwin, 1993).

Because data sets for each new structure included tubes with several helical symmetries, real-space averaging was required for calculating the final structure (Zhang et al., 1998; Yonekura and Toyoshima, 2000). For averaging in 3D, maps were calculated for each helical symmetry and cross-correlation was used to determine their relative magnifications and spatial alignment. Density scale factors were determined by linear regression of densities from corresponding pixels in the 3D maps. Individual molecules within each map were then masked, weighted according to the number of molecules contributing to the map, and averaged in real space.

Difference analysis

Comparisons were made among six different structures, namely three control Ca^{2+}-ATPase structures and three structures of Ca^{2+}-ATPase co-reconstituted with three different PLB species: PLB_{WT}, PLB_{L37A}, and PLB_{N27A}. Alignment and scaling of individual maps used the same methods as real-space averaging, and the PLB_{N27A} map was used as an align-

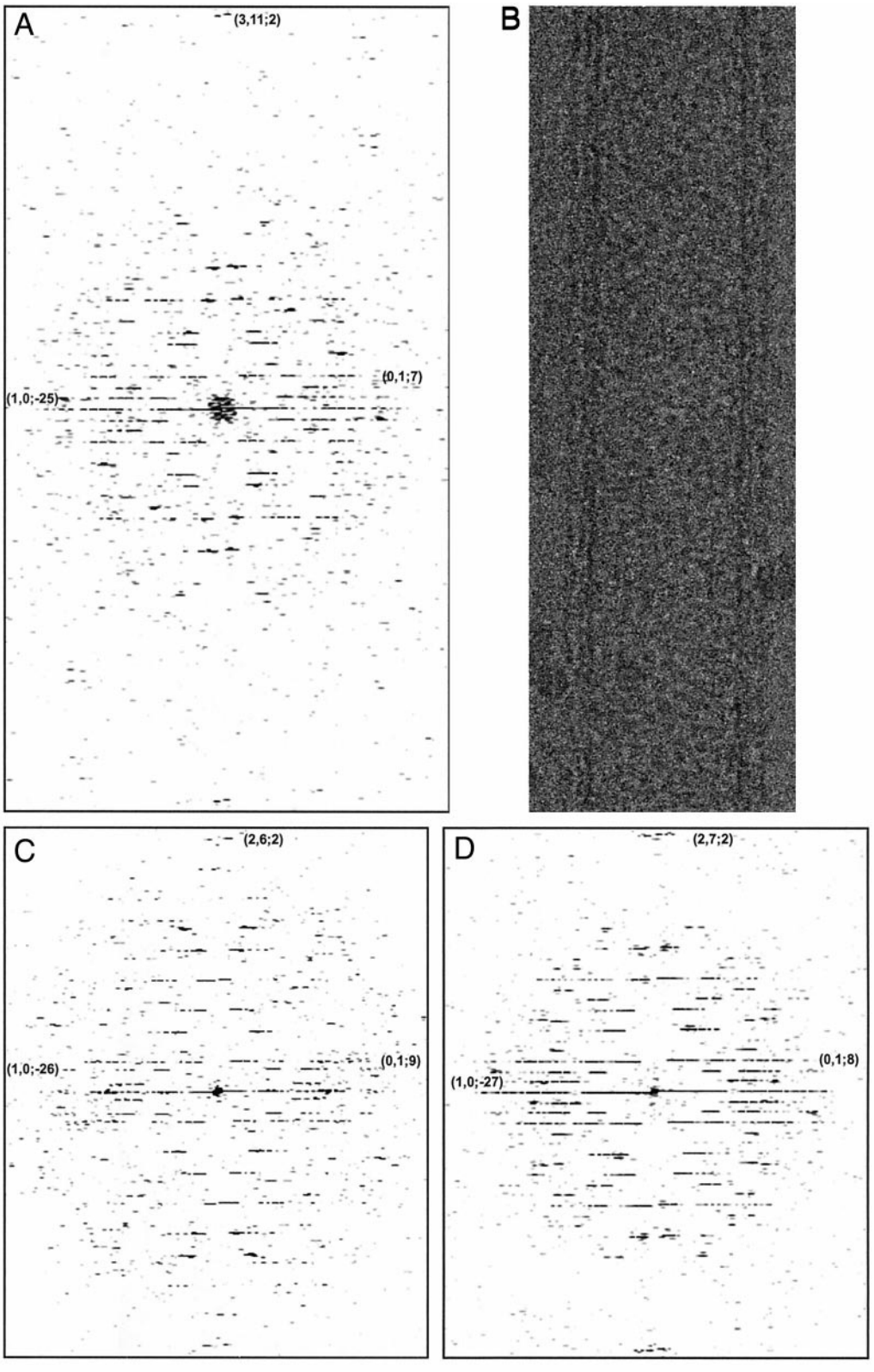

FIGURE 2 Representative data from individual frozen-hydrated tubular co-crystals. (*A*) Computed diffraction from PLB_{L37A}. (*B*) Image of PLB_{L37A} tubular co-crystal that is 700 Å in diameter. (*C*) Diffraction from PLB_{N27A}. (*D*) Diffraction from PLB_{WT}. The principal layer lines and a high-order layer line are identified by their (*h*, *k*; *n*) indices, where *h*, *k* correspond to Miller indices and *n* corresponds to the helical start number (Bessel order). Equivalent layer lines in the diffraction patterns have the same *h*, *k* indices, but differing *n*, owing to variability in the helical symmetry; the (2, k; 2) layer lines correspond to ~15 Å resolution, and the (3, 11; 2) layer line corresponds to ~10 Å resolution.

TABLE 2 Statistics for data analysis

	Control			Phospholamban		
	Native*	TG*	DTG†	WT	N27A	L37A
Oligomeric species	None	None	None	Pentamer	Pentamer	Monomer
Molar ratio				5:1	3.5:1	1:1
No. of crystals	16	7	23	14	32	23
Helical symmetries	3	1	3	2	2	6
Tube diameter	~700 Å	~600 Å	~600 Å	~700 Å	~700 Å	~700 Å
Reference symmetry	−26, 7	−22, 6	−22, 6	−27, 8	−27, 9	−26, 8
No. of molecules	40,298	21,108	51,744	29,146	86,197	53,594
Twofold phase statistics (°)§						
40 Å	1.2	3.9	1.4	1.4	0.7	1.7
30 Å	3.0	5.5	2.2	3.6	1.7	2.9
20 Å	16.5	11.2	6.2	11.6	3.8	7.1
14 Å	31.0	35.2	18.0	30.7	12.5	22.4
10 Å	43.5	41.1	32.2	42.1	23.8	33.8
8 Å	—	—	41.8	—	38.8	—
Overall	21.3	24.1	20.4	20.2	11.6	15.0
Correlation coefficients for real-space alignment¶						
	0.92	0.91	0.93	0.91	Reference	0.95

*Previously described by Young et al. (2001).
†Previously described by Zhang et al. (1998).
§Amplitude-weighted phase residuals for twofold symmetry including 100% of the off-equatorial data for the indicated resolution ranges. Random phases produce a phase residual of 45°.
¶Cross-correlation coefficients range from 0 (uncorrelated) to 1 (perfect correlation).

ment reference because it possessed the best signal-to-noise ratio as indicated by twofold phase statistics (Table 2). After alignment and density scaling, all possible combinatorial difference maps were calculated by a simple pixel-by-pixel subtraction (Yonekura et al., 1997).

When the twofold symmetry of the PLB-containing maps was not enforced, PLB appeared to occupy only one of the twofold-related sites. This asymmetry in PLB occupancy was not readily apparent in the twofold phase statistics, which are dominated by the 18-fold larger Ca^{2+}-ATPase molecules. Nevertheless, the lack of twofold symmetry in difference maps prompted us to consider the polarity of the helical lattice. In the case of PLB_{N27A}, the better signal-to-noise ratio allowed us to detect the up-down orientation of individual tubular crystals and 14 of the 32 tubular crystals were thus inverted relative to their initial orientation. Even this procedure did not fully recover PLB densities because of the following possible effects: 1) determination of tube polarity was not 100% accurate; 2) the occupancy of PLB was <100%; or 3) PLB sometimes bound at the alternate site in the unit cell, producing partial occupancy at both sites and a consequent smearing of density.

RESULTS

Functional association between PLB and Ca^{2+}-ATPase

ATPase activity was used to assess the functional interaction between PLB and Ca^{2+}-ATPase before crystallization (Table 1). The inhibitions produced by the PLB mutants N27A and L37A were quite high, with ~80% inhibition at 0.15 μM Ca^{2+}. Consistent with previous studies, this inhibition was relieved either by increased Ca^{2+} concentration (4.0 μM) or by a monoclonal antibody to PLB (2D12), which has been previously shown to mimic the effects of phosphorylation (Briggs et al., 1992; Cantilina et al., 1993; Morris et al., 1991; Sham et al., 1991; Reddy et al., 1996).

Tubular crystallization

Although the effects of decavanadate and EGTA are primarily responsible for crystallization of Ca^{2+}-ATPase, addition of PLB greatly increased the number of tubular crystals. Plausible explanations for this phenomenon are that PLB 1) stabilizes the E_2 conformation of Ca^{2+}-ATPase (Tada et al., 1980; Cantilina et al., 1993; Antipenko et al., 1997); 2) increases vesicle aggregates from which protein can be recruited and tubes can grow (Young et al., 1997); or 3) affects the physical properties of the membrane similar to fusigenic peptides (Glaser et al., 1999). At a 5:1 molar ratio (Ca^{2+}-ATPase/PLB), all PLB species produced tubular crystals that were easily disordered as they were prepared for cryoelectron microscopy. However, a 1:1 molar ratio of monomeric PLB_{L37A} produced the best-ordered tubes (Fig. 2, *a* and *b*). Lowering the ratio of pentameric PLB_{N27A} to ~3.5:1 also produced well-ordered tubes (Fig. 2 *c*). This suggests that this disorder might be due to an excess PLB in the membrane. Even though the 5:1 molar ratio used for PLB_{WT} produced more disorder, sufficient numbers of reasonably ordered tubes were eventually obtained for 3D reconstruction (Fig. 2 *d*). The anti-PLB monoclonal antibody, 2D12, inhibited tube formation if added at the outset, or disrupted existing tubular crystals if added later on, probably due to steric hindrance of crystal contacts.

3D structure of co-crystals

Three independent structures were determined for Ca^{2+}-ATPase in association with each of the PLB constructs, and

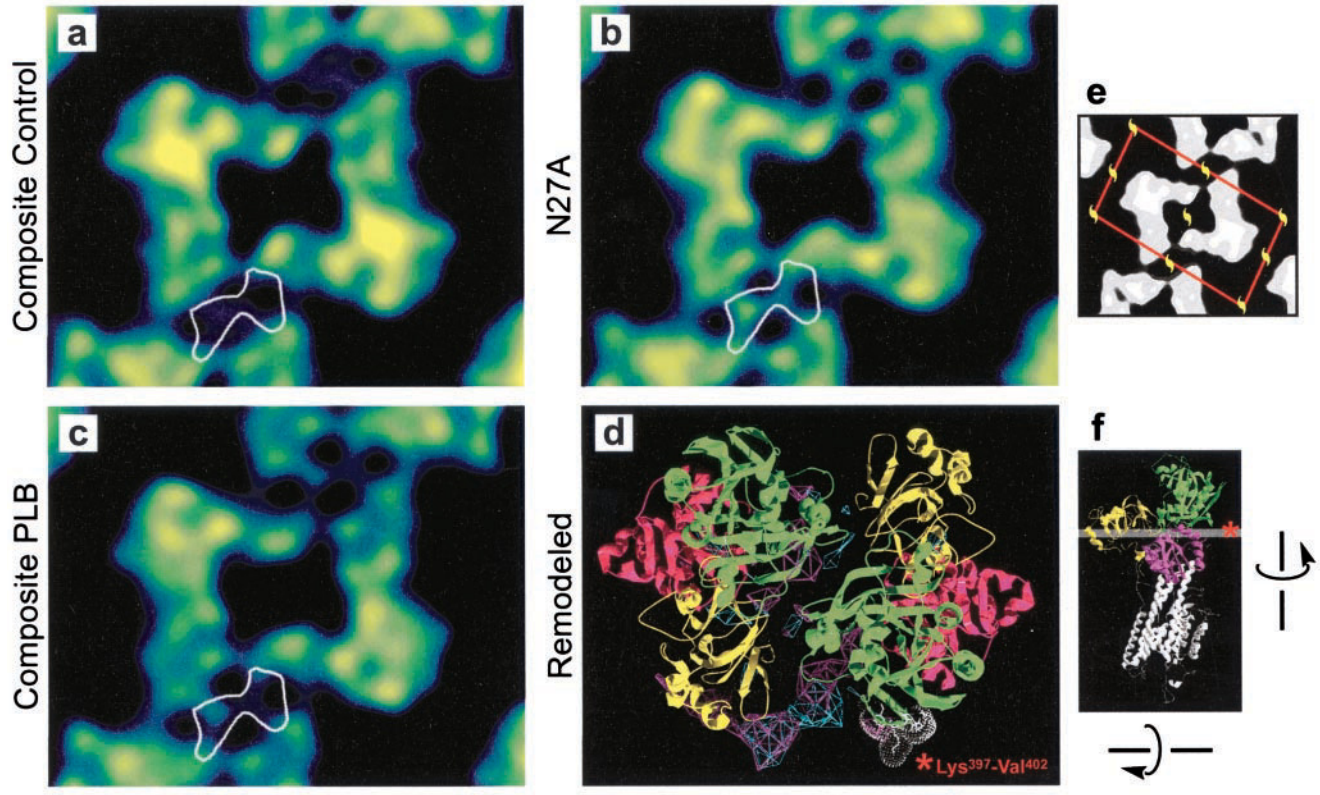

FIGURE 3 Sections through the helical reconstructions parallel to the membrane plane. (*a*) Composite control; (*b*) PLB_{N27A}; (*c*) composite PLB; (*d*) atomic model viewed from the same orientation. (*e*) The unit cell containing two molecules is shown in red with twofold axes in yellow. (*f*) Side view of the atomic model with a gray bar at the level of the sections; the arrows indicate two 90° rotations required to bring this side view to the same orientation as the left-most Ca^{2+}-ATPase molecule in the sections. The white outline in (*a*–*c*) corresponds to the 2.75 σ contour from the PLB_{N27A} difference map, though the equivalent density at the next unit cell has not been outlined. The atomic coordinates in (*d*) and (*f*) are color-coded according to domain: A (*yellow*), N (*green*), and P (*magenta*) transmembrane, stalk, and lumenal domains are white. The blue and purple surfaces in (*d*) correspond to difference densities at 2.75 σ from PLB_{N27A} and composite PLB maps, respectively. Also, the side chains and solvent-accessible surface of the PLB binding loop (Lys^{397}-Val^{402}) are colored white in (*d*).

each was compared to native Ca^{2+}-ATPase structures: $Control_{native}$ (no additives), $Control_{TG}$ (Young et al., 2001), and $Control_{DTG}$ (Zhang et al., 1998). Twofold phase statistics (Table 2) indicated that the PLB_{N27A} reconstruction extended to at least 8 Å resolution, while the PLB_{wt} and PLB_{L37A} structures extended to at least 10 Å resolution. Similarly, $Control_{native}$ and $Control_{TG}$ structures extended to 10 Å, whereas $Control_{DTG}$ extended to 8 Å resolution. The structure of Ca^{2+}-ATPase itself was indistinguishable in these six maps. In particular, the disposition of the 3 cytoplasmic domains and of the 10 transmembrane helices appeared to be identical to previous analyses (Young et al., 2001; Zhang et al., 1998; Stokes et al., 1999; Stokes and Green, 2000; Toyoshima et al., 2000).

Upon closer examination of the entire unit cell, two features were revealed that correlated with the presence of PLB. Although somewhat weak and inconsistent with the expected twofold symmetry of the crystals, these features were similar irrespective of the molar ratio or the oligomeric species of PLB. This observation led us to look for asymmetry of individual tubes. Because PLB is 18 times smaller than Ca^{2+}-ATPase, its asymmetry in the unit cell has a relatively small impact on twofold phase statistics. Also, this asymmetry implies that PLB occupies only one of two possible positions in the unit cell, and this position must be consistent throughout the tube to affect phase statistics: random positioning of PLB at either of the two possible binding sites would simply smear out its density in the final map. Either because of the innately low signal or because of different levels of consistency or occupancy, we could only detect individual tube asymmetry in the highest resolution data set (N27A). Thus, although the same densities are observed in the other PLB data sets, they are reduced due to averaging of unit cells with PLB in alternate positions. In an attempt to maximize the signal-to-noise ratio, we generated composite maps in the presence and absence of PLB by weighted averaging of the control structures (Native, TG, and DTG) and PLB structures (WT, L37A, and N27A) in real space. Sections through N27A and composite PLB maps reveal a relatively strong density not present in the

control maps (Fig. 3). Other sections at the surface of the membrane (not shown) reveal continuous density adjacent to the cytoplasmic regions of Ca^{2+}-ATPase transmembrane segments M1, M2, and M3. Surprisingly, there were no extra densities that could be assigned to the transmembrane domain of PLB.

Difference maps

To quantitate structural differences in the presence of PLB, the six maps were limited to 10 Å resolution, aligned in real space, and densities were subtracted to produce difference maps. In pair-wise comparisons, the two highest resolution structures, namely $Control_{DTG}$ and PLB_{N27A}, resulted in the strongest and cleanest difference map, owing to the higher signal-to-noise ratio and to our ability to detect the asymmetry of individual PLB_{N27A} tubes (Fig. 4 *a*). The difference map is contoured at 2.75 σ of the distribution of difference densities for both positive and negative differences. When viewed in 3D, these difference densities compose a column, which bridges the nose (A) and nucleotide-binding (N) domains of neighboring Ca^{2+}-ATPase molecules, and an arc at the membrane interface of M1, M2, and M3. This arc appears to extend over toward the neighboring Ca^{2+}-ATPase molecule, but does not actually make contact with it. The only large negative differences are associated with the intramolecular decavanadate site in the cytoplasmic domain (Stokes and Green, 2000; Toyoshima et al., 2000) and with the TG binding site at the tip of the lumenal domain (Young et al., 2001). These negative densities reflect the lack of TG in the PLB_{N27A} tubes and a lower occupancy of decavanadate.

In addition to PLB_{N27A}-$Control_{DTG}$, all pair-wise combinatorial difference maps were generated from the structures described in Table 2. The nine difference maps in the presence of PLB are shown in Fig. 4 *b*. Difference maps from PLB_{WT} and PLB_{L37A} are expected to be noisier because the asymmetry of individual tubes could not be detected. Nevertheless, positive differences dominated the gallery of difference maps in two locations: one in the cytoplasmic domain (six of the nine difference maps) and one at the surface of the membrane (three of the nine difference maps). Both differences were present in the higher-resolution difference map from PLB_{N27A}-$Control_{DTG}$. Only one of the nine difference maps (PLB_{WT}-$Control_{TG}$) showed neither feature, likely due to the fact that both of these data sets contained the smallest number of tubular crystals, and therefore the highest level of noise.

These other structures are represented in the difference map between the composite PLB and composite Control structures. Small differences in scaling required that the upper and lower portions of the maps be re-aligned independently. The resulting map indicates that differences from PLB_{WT} and PLB_{L37A} structures are consistent with those from PLB_{N27A}.

DISCUSSION

Interpretation of difference maps

In the current work, three different PLB constructs were co-reconstituted with Ca^{2+}-ATPase. After demonstrating a functional interaction, co-crystals were grown and three separate structures for the PLB/Ca^{2+}-ATPase inhibitory complex were determined. The structure of Ca^{2+}-ATPase itself appears unaffected by the presence of PLB, but consistent difference densities were observed adjacent to Ca^{2+}-ATPase. We believe these difference densities are consistent with a particular model for the cytoplasmic domain of PLB and suggest a mode for binding and inhibition. However, this interpretation is not straightforward due to the discontinuity of difference densities and their absence from the membrane domain. Therefore, we will first discuss the features of our difference map to justify our assignments and modeling of PLB.

The most likely explanation for the discontinuous difference densities is a high level of noise in the difference map. At lower thresholds these densities are continuous, but are also accompanied by numerous other discontinuous densities spread throughout the map. Even at the relatively high threshold in Fig. 4, various inconsistent peaks appear in the gallery of individual difference maps (Fig. 4 *b*). Given this limitation in the signal-to-noise ratio, we believe that a comparison of the individual difference maps (Fig. 4 *b*) provides a way to distinguish real difference peaks from noise. The composite structure in Fig. 4 *c* does this to some extent, but does not distinguish whether the density labeled "IB" continues horizontally toward the blue Ca^{2+}-ATPase molecule or upward to connect with the density labeled "IA." We favor the latter interpretation, because the rightmost density (labeled "?") is only present in one individual difference map, whereas "IA" is present in six maps. It is possible that this "?" density represents an alternative location for PLB domain IA, or a partially occupied site for a second PLB molecule within the unit cell; however, the fact that this "?" density is not in physical contact with the blue Ca^{2+}-ATPase molecule means that these alternatives probably do not represent the physiological binding mode for PLB. In the transmembrane domain no plausible densities are seen at all, leading us to conclude that the transmembrane helix of PLB is disordered in our crystals.

Previous models for PLB

Two basic alternatives have previously been proposed for the structure of PLB. Both agree that the N-terminal domain IA (residues 1–16) and the transmembrane domain II (residues 33–52) are α-helical. The remaining domain IB (residues 17–32) has been alternately described as an α-helix (Arkin et al., 1995; Pollesello et al., 1999; Lamberth et al., 2000) or as a relatively unstructured loop (Tatulian et al.,

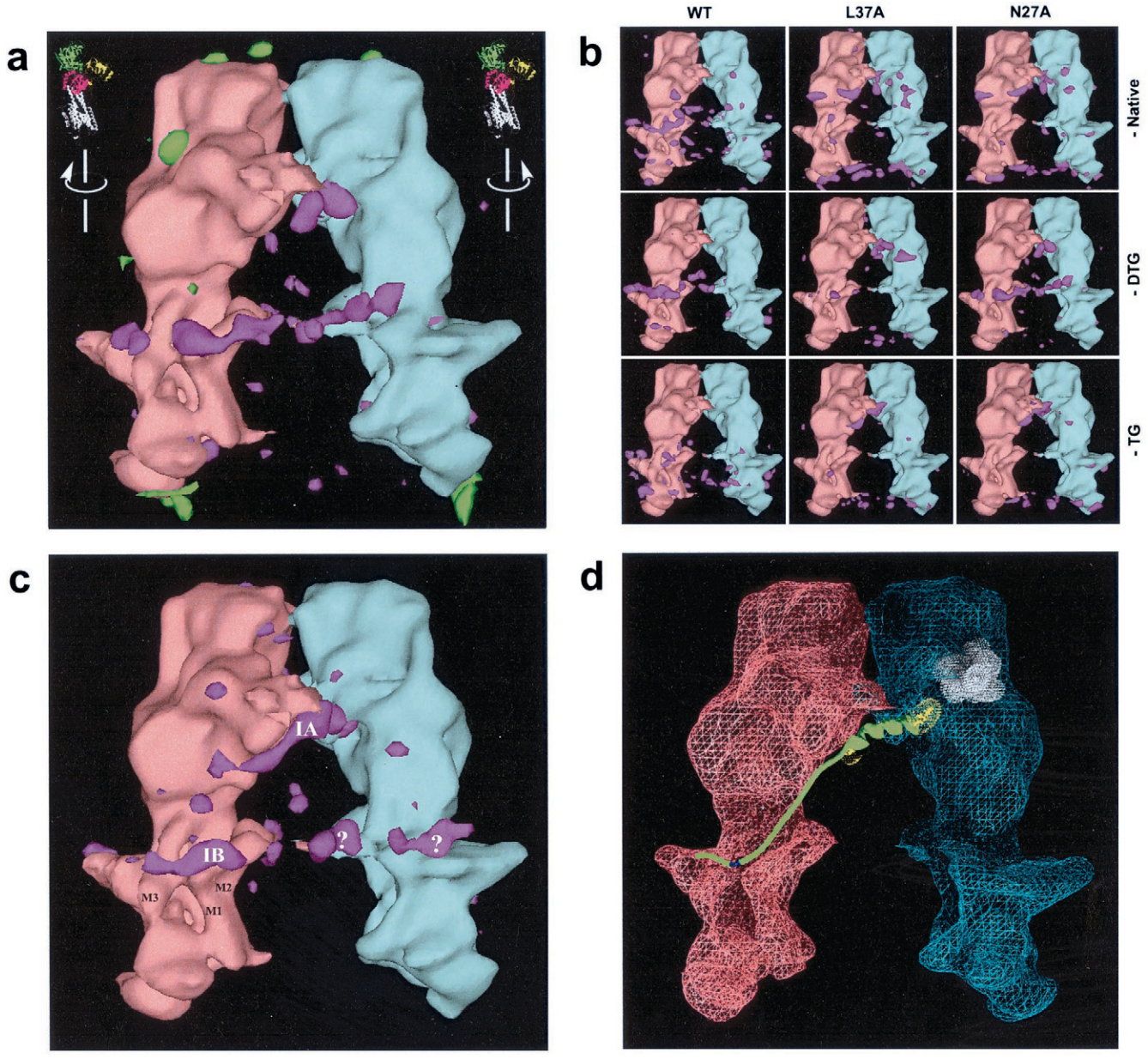

FIGURE 4 Difference maps overlaid on two Ca^{2+}-ATPase molecules from the crystal lattice. (*a*) Difference densities from PLB_{N27A}-$Control_{DTG}$ are rendered at 2.75 σ; positive differences are purple and negative differences are green. (*b*) The nine individual difference maps among the three control reconstructions (Native, DTG, and TG) and the three PLB reconstructions (WT, L37A, and N27A), showing positive differences at 2.75 σ. (*c*) Difference densities from composite PLB-composite Control structures at 2.75 σ; labels indicate our assignments to PLB cytoplasmic domains and M1, M2, and M3 transmembrane helices of Ca^{2+}-ATPase. (*d*) Model for a PLB monomer interacting with two Ca^{2+}-ATPase molecules. PLB domain IA (residues 1–16) is helical and links the A and N domains of neighboring Ca^{2+}-ATPase molecules. PLB domain IB (residues 17–32) is unstructured and extends ~58 Å to make contact with the interfacial regions of M1-M3. The solvent-accessible surfaces of PLB's Lys^{3} and Ser^{16} are yellow, whereas those of Ca^{2+}-ATPase's Lys^{397}-Val^{402} are white; the C_α position of Asn^{27} is colored blue. Orientations of the pink and blue Ca^{2+}-ATPase molecules are shown in the upper corners of (*a*).

1995; Simmerman et al., 1989; Vorherr et al., 1993; Terzi et al., 1992; Mortishire-Smith et al., 1995). This discrepancy may be a result of solvent conditions, given that the FTIR and CD studies supporting the loop used physiological buffers, whereas the NMR studies revealing a helix used either high concentrations of trifluoroethanol or a mixture of chloroform/methanol.

Interaction of these domains with Ca^{2+}-ATPase has been characterized by mutagenesis and, in one case, by chemical cross-linking. One of the most important interactions appears to be between the N-terminus of PLB and the Ca^{2+}-ATPase loop Lys^{397}-Val^{402} (Toyofuku et al., 1993, 1994; Kimura et al., 1998a). In particular, mutagenesis of either PLB domain IA or this Ca^{2+}-ATPase loop abolishes the

inhibitory capacity of PLB, and also the ability to coimmunoprecipitate Ca^{2+}-ATPase with an anti-PLB antibody (Asahi et al., 2000). These studies are consistent with cross-linking of the Ca^{2+}-ATPase loop to Lys^3 of PLB in a Ca^{2+}-dependent manner (James et al., 1989). Interaction of domain IB with Ca^{2+}-ATPase is supported by the enhanced inhibitory capacity of the N27A and N30A mutants, which unlike the mutations in membrane domain II do not affect the oligomeric state of PLB (Kimura et al., 1998b).

Our model for PLB

Using these interaction sites as constraints, we have built a model for the cytoplasmic domain of PLB based on our difference map. In particular, the difference density labeled IA forms a cylinder ~10 Å in diameter and 25 Å long, and is thus compatible with the N-terminal helix of PLB (domain IA). Furthermore, after placing the N-terminal helix into this density, the Lys^{397}-Val^{402} loop on Ca^{2+}-ATPase lies 9 Å from Lys^3 on PLB, which is well within cross-linking distance, especially considering that the corresponding domain of Ca^{2+}-ATPase (N domain) is able to move up to 50 Å (Toyoshima et al., 2000). The domain IA density dwindles somewhere between Thr^{17} and Pro^{21}, which is consistent both with the NMR structures (Mortishire-Smith et al., 1995; Arkin et al., 1995; Pollesello et al., 1999; Lamberth et al., 2000) and with predictions of secondary structure (Tatulian et al., 1995; Simmerman et al., 1989; Vorherr et al., 1993; Terzi et al., 1992). When modeled as an extended chain, domain IB is long enough to run through the correspondingly labeled difference density, thus placing Asn^{27} of PLB next to the cytoplasmic extension of M1 and M3 of Ca^{2+}-ATPase. The lack of twofold symmetry in our difference maps suggests a stoichiometry of only one PLB to two Ca^{2+}-ATPase molecules.

According to the most recent NMR structure (Lamberth et al., 2000), PLB might be modeled as a single, long α-helix with flexibility between Thr^{17} and Met^{20}. This helix would be just long enough to reach from a transmembrane position adjoining M6 to the Lys^{397}-Val^{402} loop. This alternative model is consistent with mutagenesis (Asahi et al., 1999) and co-immunoprecipitation (Asahi et al., 2000) studies supporting an interaction between PLB domain II and Ca^{2+}-ATPase M6. However, we have observed no difference densities that are consistent with this alternative, either next to the cytoplasmic domain or within the membrane. Instead, our model suggests that PLB domain II may enter the membrane near M3. Unlike the unhindered region adjacent to M6, there is a crystal contact at the lumenal side of M3, which could explain the disordering of the PLB transmembrane domain in our co-crystals. This hypothesis requires that M6 mutations exert an indirect influence over PLB binding. Indeed, three of five sensitive M6 residues are buried in the atomic structure, supporting the relevance of indirect effects regardless of where PLB binds.

Functional implications of our model

PLB appears to bind preferentially to the E_2 conformation of Ca^{2+}-ATPase (James et al., 1989; Asahi et al., 2000) and kinetic studies have specifically attributed PLB inhibition to a slowing either of the Ca^{2+}-induced transition from E_2 to E_1 (Cantilina et al., 1993) or of E_2-P hydrolysis (Sasaki et al., 1992; Antipenko et al., 1997). The catalytic cycle of Ca^{2+}-ATPase uses dramatic domain motions that have been recently characterized by comparing the x-ray crystal structure of the $E_1 \cdot Ca_2$ conformation (Toyoshima et al., 2000) with the EM structure, which appears to represent either the E_2 (Stokes and Lacapere, 1994) or the E_2-P conformation (Danko et al., 2001). The most dramatic movement involves a 90° rotation of the A domain, though the P domain also rotates by 45° and the N domain is translated by as much as 50 Å (Toyoshima et al., 2000; Rice, Xu, and Stokes, unpublished results). According to our model, PLB links the A and N domains of adjacent Ca^{2+}-ATPase molecules and could therefore inhibit Ca^{2+}-ATPase by resisting these domain motions. Depending on the particular Ca^{2+}-ATPase conformation stabilized by PLB (E_2 or E_2-P), binding could inhibit either E_2-P hydrolysis, the Ca^{2+}-induced E_2 to E_1 transition, or perhaps both.

Inhibition by PLB is relieved either by phosphorylation of Ser^{16} or by elevated Ca^{2+} concentrations. In our model, Ser^{16} faces the A-domain of Ca^{2+}-ATPase at the end of domain IA (Fig. 4 *d*) and several studies indicate that phosphorylation causes partial unwinding of the N-terminal helix (Tatulian et al., 1995; Simmerman et al., 1989; Terzi et al., 1992; Mortishire-Smith et al., 1995). Such unwinding could destabilize this intermolecular interaction and thus allow the A domain to undergo the necessary movements for catalysis. If PLB binding to adjacent molecules required that they both be in the same state (e.g., E_2), then an increased rate of Ca^{2+}-ATPase turnover would reduce the probability of simultaneously finding these molecules in this state. Thus, PLB binding would be sensitive to the kinetics of Ca^{2+}-ATPase, which could account for the observed Ca^{2+} dependence of PLB inhibition.

The authors acknowledge Rameen Berkhouim, Nigel Unwin, Chikashi Toyoshima, and Koji Yonekura for developing and sharing the computer programs we used for image analysis and determination of difference maps.

This work was supported by National Institutes of Health Grant R01 GM56960 (to D.L.S.) and Scientist Development Grant 9930278T from the American Heart Association, Heritage Affiliate (to H.S.Y.). In the initial stages of this work H.S.Y. was supported by National Institutes of Health National Research Service Award F32 GM18281.

REFERENCES

Antipenko, A., A. Spielman, M. Sassaroli, and M. Kirchberger. 1997. Comparison of the kinetic effects of phospholamban phosphorylation and anti-phospholamban monoclonal antibody on the calcium pump in

purified cardiac sarcoplasmic reticulum membranes. *Biochemistry.* 36: 12903–12910.

Arkin, I. T., M. Rothman, C. F. C. Ludlam, S. Aimoto, D. M. Engelman, K. J. Rothschild, and S. O. Smith. 1995. Structural model of the phospholamban ion channel complex in phospholipid membranes. *J. Mol. Biol.* 248:824–834.

Asahi, M., Y. Kimura, K. Kurzydlowski, M. Tada, and D. MacLennan. 1999. Transmembrane helix M6 in sarco(endo)plasmic reticulum Ca^{2+}-ATPase forms a functional interaction site with phospholamban. Evidence for physical interactions at other sites. *J. Biol. Chem.* 274: 32855–32862.

Asahi, M., E. McKenna, K. Kurzydlowski, M. Tada, and D. MacLennan. 2000. Physical interactions between phospholamban and sarco(endo)-plasmic reticulum Ca^{2+}-ATPases are dissociated by elevated Ca^{2+}, but not by phospholamban phosphorylation, vanadate, or thapsigargin, and are enhanced by ATP. *J. Biol. Chem.* 275:15034–15038.

Auer, M., G. Scarborough, and W. Kuhlbrandt. 1998. Three-dimensional map of the plasma membrane H^+-ATPase in the open conformation. *Nature.* 392:840–843.

Autry, J., and L. Jones. 1997. Functional co-expression of the canine cardiac Ca^{2+} pump and phospholamban in *Spodoptera frugiperda* (Sf21) cells reveals new insights on ATPase regulation. *J. Biol. Chem.* 272:15872–15880.

Beroukhim, R., and N. Unwin. 1997. Distortion correction of tubular crystals: improvements in the acetylcholine receptor structure. *Ultramicroscopy.* 70:57–81.

Briggs, F. N., K. F. Lee, A. W. Wechsler, and L. R. Jones. 1992. Phospholamban expressed in slow-twitch and chronically stimulated fast-twitch muscles minimally affects calcium affinity of sarcoplasmic reticulum Ca-ATPase. *J. Biol. Chem.* 267:26056–26061.

Cantilina, T., Y. Sagara, G. Inesi, and L. R. Jones. 1993. Comparative studies of cardiac and skeletal sarcoplasmic reticulum ATPases: effect of phospholamban antibody on enzyme activation. *J. Biol. Chem.* 268: 17018–17025.

Chen, P. S., T. Y. Toribara, and H. Warner. 1956. Microdetermination of phosphorous. *Anal. Chem.* 28:1756–1758.

Chester, D. W., L. G. Herbette, R. P. Mason, A. F. Joslyn, and D. J. Triggle. 1987. Diffusion of dihydropyridine calcium channel antagonists in cardiac sarcolemmal lipid multibilayers. *Biophys. J.* 52:1021–1030.

Cornea, R., J. Autry, Z. Chen, and L. Jones. 2000. Re-examination of the role of the leucine/isoleucine zipper residues of phospholamban in inhibition of the Ca^{2+}-pump of cardiac sarcoplasmic reticulum. *J. Biol. Chem.* 275:41487–41494.

Cornea, R. L., L. R. Jones, J. M. Autry, and D. D. Thomas. 1997. Mutation and phosphorylation change the oligomeric structure of phospholamban in lipid bilayers. *Biophys. J.* 36:2960–2967.

Danko, S., T. Daiho, K. Yamasaki, M. Kamidochi, H. Suzuki, and C. Toyoshima. 2001. ADP-insensitive phosphoenzyme intermediate of sarcoplasmic reticulum Ca^{2+}-ATPase has a compact conformation resistant to proteinase K, V8 protease and trypsin. *FEBS Lett.* 489:277–282.

DeRosier, D. J., and P. B. Moore. 1970. Reconstruction of three-dimensional images from electron micrographs of structures with helical symmetry. *J. Mol. Biol.* 52:355–369.

Dux, L., and A. Martonosi. 1983. Two-dimensional arrays of proteins in sarcoplasmic reticulum and purified Ca^{2+}-ATPase vesicles treated with vanadate. *J. Biol. Chem.* 258:2599–2603.

Eletr, S., and G. Inesi. 1972. Phospholipid orientation in sarcoplasmic reticulum membranes: spin-label ESR and proton NMR studies. *Biochim. Biophys. Acta.* 282:174–179.

Fabiato, A., and F. Fabiato. 1979. Calculator programs for computing the composition of the solutions containing multiple metals and ligands used for experiments in skinned muscle cells. *J. Physiol.* 75:463–505.

Glaser, R., M. Grune, C. Wandelt, and A. Ulrich. 1999. Structure analysis of a fusogenic peptide sequence from the sea urchin fertilization protein binding. *Biochemistry.* 38:2560–2569.

Hasenfuss, G. 1998. Calcium pump overexpression and myocardial function. Implications for gene therapy of myocardial failure. *Cardiovasc. Res.* 37:279–289.

James, P., M. Inui, M. Tada, M. Chiesi, and E. Carafoli. 1989. Nature and site of phospholamban regulation of the Ca^{2+} pump of sarcoplasmic reticulum. *Nature.* 342:90–92.

Jorgensen, P. L., and J. P. Andersen. 1988. Structural basis for E1–E2 conformational transitions in Na, K-pump and Ca-pump proteins. *J. Membr. Biol.* 103:95–120.

Kimura, Y., M. Asahi, K. Kurzydlowski, M. Tada, and D. MacLennan. 1998a. Amino acids Lys-Asp-Asp-Lys-Pro-Val402 in the Ca^{2+}-ATPase of cardiac sarcoplasmic reticulum are critical for functional association with phospholamban. *J. Biol. Chem.* 273:14238–14241.

Kimura, Y., M. Asahi, K. Kurzydlowski, M. Tada, and D. H. MacLennan. 1998b. Phospholamban domain Ib mutations influence functional interactions with the Ca^{2+}-ATPase isoform of cardiac sarcoplasmic reticulum. *J. Biol. Chem.* 273:14238–14241.

Kimura, Y., K. Kurzydlowski, M. Tada, and D. MacLennan. 1996. Phospholamban regulates the Ca^{2+}-ATPase through intramembrane interactions. *J. Biol. Chem.* 271:21726–21731.

Kimura, Y., K. Kurzydlowski, M. Tada, and D. H. MacLennan. 1997. Phospholamban inhibitory function is enhanced by depolymerization. *J. Biol. Chem.* 272:15061–15064.

Kirchberger, M. A., M. Tada, and A. M. Katz. 1974. Adenosine 3′:5′-monophosphate-dependent protein kinase catalyzed phosphorylation reaction and its relationship to calcium transport in cardiac sarcoplasmic reticulum. *J. Biol. Chem.* 249:6166–6173.

Lamberth, S., H. Schmid, M. Muenchbach, T. Vorherr, J. Krebs, E. Carafoli, and C. Griesinger. 2000. NMR solution structure of phospholamban. *Helvetica Chimica Acta.* 83:2141–2152.

Levy, D., A. Bluzat, M. Seigneuret, and J.-L. Rigaud. 1990a. A systematic study of liposome and proteoliposome reconstitution involving Bio-Bead-mediated Triton X-100 removal. *Biochim. Biophys. Acta.* 1025: 179–190.

Levy, D., A. Gulik, M. Seigneuret, and J.-L. Rigaud. 1990b. Phospholipid vesicle solubilization and reconstitution by detergents. Symmetrical analysis of the two processes using octaethylene glycol mono-n-dodecyl ether. *Biochemistry.* 29:9480–9488.

Lowry, O. H., N. J. Rosebrough, A. L. Farr, and R. J. Randall. 1951. Protein measurement with the folin phenol reagent. *J. Biol. Chem.* 193:265–275.

Luo, W., I. L. Grupp, J. Harrer, S. Ponniah, G. Grupp, J. J. Duffy, T. Doetschman, and E. G. Kranias. 1994. Targeted ablation of the phospholamban gene is associated with markedly enhanced myocardial contractility and loss of α-agonist stimulation. *Circ. Res.* 75:401–409.

Markwell, M. H., S. M. Hass, L. L. Beiber, and N. E. Tolbert. 1978. A modification of the Lowry procedure to simplify protein determination in membrane and lipoprotein samples. *Anal. Biochem.* 87:206–210.

Meyer, M., W. Schillinger, B. Pieske, C. Holubarsch, C. Heilmann, H. Posival, G. Kuwajima, K. Mikoshiba, H. Just, and G. Hasenfuss. 1995. Alterations of sarcoplasmic reticulum proteins in failing human dilated cardiomyopathy. *Circulation.* 92:778–784.

Minmamisawa, S., M. Hoshijima, G. Chu, C. Ward, K. Frank, Y. Gu, M. Martone, Y. Wang, J. Ross, E. Kranias, W. Giles, and K. Chien. 2000. Chronic phospholamban-sarcoplasmic reticulum calcium ATPase interaction is the critical calcium cycling defect in dilated cardiomyopathy. *Cell.* 99:313–322.

Morris, G. L., H. Cheng, J. Colyer, and J. H. Wang. 1991. Phospholamban regulation of cardiac sarcoplasmic reticulum (Ca^{2+}-Mg^{2+})-ATPase: mechanism of regulation and site of monoclonal antibody interaction. *J. Biol. Chem.* 266:11270–11275.

Mortishire-Smith, R. J., S. M. Pitzenberger, C. J. Burke, C. R. Middaugh, V. M. Garsky, and R. G. Johnson. 1995. Solution structure of the cytoplasmic domain of phospholamban: phosphorylation leads to a local perturbation of secondary structure. *Biochemistry.* 34:7603–7613.

Pollesello, P., A. Annila, and M. Ovaska. 1999. Structure of the 1–36 amino-terminal fragment of human phospholamban by nuclear magnetic resonance and modeling of the phospholamban pentamer. *Biophys. J.* 76:1784–1795.

Reddy, L., J. Autry, L. Jones, and D. Thomas. 1999. Co-reconstitution of phospholamban mutants with the Ca-ATPase reveals dependence of

inhibitory function on phospholamban structure. *J. Biol. Chem.* 274: 7649–7655.

Reddy, L. G., L. R. Jones, S. E. Cala, J. J. O'Brian, S. A. Tatulian, and D. L. Stokes. 1995. Functional reconstitution of recombinant phospholamban with rabbit skeletal Ca-ATPase. *J. Biol. Chem.* 270:9390–9397.

Reddy, L. G., L. R. Jones, R. C. Pace, and D. L. Stokes. 1996. Purified, reconstituted cardiac Ca^{2+}-ATPase is regulated by phospholamban but not by direct phosphorylation with Ca^{2+}/calmodulin-dependent protein kinase. *J. Biol. Chem.* 271:14964–14970.

Sagara, Y., F. Fernandez-Belda, L. de Meis, and G. Inesi. 1992. Characterization of the inhibition of intracellular Ca^{2+} transport ATPases by thapsigargin. *J. Biol. Chem.* 267:12606–12613.

Sasaki, T., M. Inui, Y. Kimura, T. Kuzuyu, and M. Tada. 1992. Molecular mechanism of regulation of Ca^{2+} pump ATPase by phospholamban in cardiac sarcoplasmic reticulum. *J. Biol. Chem.* 267:1674–1679.

Sham, J. S. K., L. R. Jones, and M. Morad. 1991. Phospholamban mediates the beta-adrenergic-enhanced Ca^{2+} uptake in mammalian ventricular myocytes. *Am. J. Physiol. Heart Circ. Physiol.* 261:H1344–H1349.

Simmerman, H., and L. Jones. 1998. Chronic phospholamban-sarcoplasmic reticulum calcium ATPase interaction is the critical calcium cycling defect in dilated cardiomyopathy. *Physiol Rev.* 78: 921–947.

Simmerman, H. K. B., D. E. Lovelace, and L. R. Jones. 1989. Secondary structure of detergent-solubilized phospholamban, a phosphoralatable, oligomeric protein of cardiac sarcoplasmic reticulum. *Biochim. Biophys. Acta.* 997:322–329.

Sordahl, L., W. McCollum, W. Wood, and A. Schwartz. 1973. Mitochondria and sarcoplasmic reticulum function in cardiac hypertrophy and failure. *Am J. Physiol.* 224:497–502.

Stokes, D. 1997. Keeping calcium in its place: Ca^{2+}-ATPase and phospholamban. *Curr. Opin. Struct. Biol.* 7:550–556.

Stokes, D., M. Auer, P. Zhang, and W. Kuhlbrandt. 1999. Comparison of H+-ATPase and Ca^{2+}-ATPase suggests that a large conformational change initiates P-type ion pump reaction cycles. *Current Biology.* 9:672–679.

Stokes, D. L., and N. M. Green. 1990. Three-dimensional crystals of Ca-ATPase from sarcoplasmic reticulum: symmetry and molecular packing. *Biophys. J.* 57:1–14.

Stokes, D. L., and N. M. Green. 2000. Modeling a dehalogenase fold into the 8-Å density map for Ca^{2+}-ATPase defines a new domain structure. *Biophys. J.* 78:1765–1776.

Stokes, D. L., and J.-J. Lacapere. 1994. Conformation of Ca^{2+}-ATPase in two crystal forms: effects of Ca^{2+}, thapsigargin, AMP-PCP, and Cr-ATP on crystallization. *J. Biol. Chem.* 269:11606–11613.

Tada, M., M. A. Kirchberger, D. I. Repke, and A. M. Katz. 1974. The stimulation of calcium transport in cardiac sarcoplasmic reticulum by adenosine 3′:5′-monophosphate-dependent protein kinase. *J. Biol. Chem.* 249:6174–6180.

Tada, M., M. Yamada, F. Ohmori, T. Kuzuya, M. Inui, and H. Abe. 1980. Transient state kinetic studies of Ca^{2+}-dependent ATPase and calcium transport by cardiac sarcoplasmic reticulum. Effect of cyclic AMP-dependent protein kinase-catalyzed phosphorylation of phospholamban. *J. Biol. Chem.* 255:1985–1992.

Tani, K., H. Sasabe, and C. Toyoshima. 1997. A set of computer programs for determining defocus and astigmatism in electron images. *Ultramicroscopy.* 65:31–44.

Tatulian, S. A., L. R. Jones, L. G. Reddy, D. L. Stokes, and L. K. Tamm. 1995. Secondary structure and orientation of phospholamban reconstituted in supported bilayers from polarized attenuated total reflection FTIR spectroscopy. *Biochemistry.* 34:4448–4456.

Terzi, E., L. Poteur, and E. Trifilieff. 1992. Evidence for a phosphorylation-induced conformational change in phospholamban cytoplasmic domain by CD analysis. *FEBS Lett.* 309:413–416.

Toyofuku, T., K. Kurzydlowski, M. Tada, and D. H. MacLennan. 1993. Identification of regions in the Ca^{2+}-ATPase of sarcoplasmic reticulum that affect functional association with phospholamban. *J. Biol. Chem.* 268:2809–2815.

Toyofuku, T., K. Kurzydlowski, M. Tada, and D. H. MacLennan. 1994. Amino acids Glu^2 to Ile^{18} in the cytoplasmic domain of phospholamban are essential for functional association with the Ca^{2+}-ATPase of sarcoplasmic reticulum. *J. Biol. Chem.* 269:3088–3094.

Toyoshima, C., M. Nakasako, H. Nomura, and H. Ogawa. 2000. Crystal structure of the calcium pump of sarcoplasmic reticulum at 2.6 Å resolution. *Nature.* 405:647–655.

Toyoshima, C., and N. Unwin. 1990. Three-dimensional structure of the acetylcholine receptor by cryoelectron microscopy and helical image reconstruction. *J. Cell. Biol.* 111:2623–2635.

Toyoshima, C., K. Yonekura, and H. Sasabe. 1993. Contrast transfer for frozen-hydrated specimens. II. Amplitude contrast at very low frequencies. *Ultramicroscopy.* 48:165–176.

Unwin, N. 1993. Nicotinic acetylcholine receptor at 9 Å resolution. *J. Mol. Biol.* 229:1101–1124.

Vorherr, T., A. Wrzosek, M. Chiesi, and E. Carafoli. 1993. Total synthesis and functional properties of the membrane intrinsic protein phospholamban. *Protein Sci.* 2:339–347.

Warren, G. B., P. A. Toon, N. J. M. Birdsall, A. G. Lee, and J. C. Metcalfe. 1974. Reconstitution of a calcium pump using defined membrane components. *Proc. Natl. Acad. Sci. U.S.A.* 71:622–626.

Whitmer, J., P. Kumar, and R. Solaro. 1988. Calcium transport properties of cardiac sarcoplasmic reticulum from cardiomyopathic Syrian hamsters (BIO 53.58 and 14.6): evidence for a quantitative defect in dilated myopathic hearts not evident in hypertrophic hearts. *Circ. Res.* 62: 81–85.

Yonekura, K., D. L. Stokes, H. Sasabe, and C. Toyoshima. 1997. The ATP-binding site of Ca^{2+}-ATPase revealed by electron image analysis. *Biophys. J.* 72:997–1005.

Yonekura, K., and C. Toyoshima. 2000. Structure determination of tubular crystals of membrane proteins. II. Averaging of tubular crystals of different helical classes. *Ultramicroscopy.* 84:15–28.

Young, H., L. Reddy, L. Jones, and D. Stokes. 1998. Co-reconstitution and co-crystallization of phospholamban and Ca^{2+}-ATPase. *Ann. NY Acad. Sci.* 853:103–115.

Young, H. S., J. L. Rigaud, J. J. Lacapere, L. G. Reddy, and D. L. Stokes. 1997. How to make tubular crystals by reconstitution of detergent-solubilized Ca^{2+}-ATPase. *Biophys. J.* 72:2545–2558.

Young, H., C. Xu, P. Zhang, and D. Stokes. 2001. Locating the thapsigargin binding site on Ca^{2+}-ATPase by cryoelectron microscopy. *J. Mol. Biol.* 308:231–240.

Zhang, P., C. Toyoshima, K. Yonekura, N. Green, and D. Stokes. 1998. Structure of the calcium pump from sarcoplasmic reticulum at 8-Å resolution. *Nature.* 392:835–839.